PROCEEDINGS OF SCIENCE

Heavy Quarkonium from Lattice QCD

Brian Colquhoun,[a,*] **Laurence Cooper,**[a] **Christine Davies,**[a] **G. Peter Lepage**[b] **and Sophie Renner**[a]

[a] *School of Physics and Astronomy, University of Glasgow, Glasgow, G12 8QQ, UK*

[b] *Laboratory of Elementary Particle Physics, Cornell University, Ithaca, New York 14853, USA*

E-mail: brian.colquhoun@glasgow.ac.uk

We discuss recent progress in radiative decays of heavy quarkonium from 2 + 1 + 1 flavour lattice QCD using the Highly Improved Staggered Quark formalism for all quarks. In particular, we summarise our recent calculations of the decay of heavyonium mesons to on-shell photons. Our calculation of the form factor for the decay $\eta_c \to \gamma\gamma$ and the determination of its decay width has changed the theoretical picture of the process. By calculating the decay width for the process $\eta_b \to \gamma\gamma$ we have provided a robust and timely prediction for experimental searches possible at, for example, Belle II. We then explore Beyond the Standard Model physics by studying $J/\psi \to \gamma a$ where a is an axion-like particle. Our fully relativistic calculation using lattice QCD leads to precise branching fractions and exclusion limits that can now be used in place of nonrelativistic perturbative expansion results that do not fully take nonperturbative effects of hadron decays into account.

The XVIth Quark Confinement and the Hadron Spectrum Conference (QCHSC24)
19-24 August, 2024
Cairns Convention Centre, Cairns, Queensland, Australia

*Speaker

 ISSN 1824-8039 . Published by SISSA Medialab.

PoS(QCHSC24)120

1. Introduction

In these proceedings we report on recent heavy quarkonium calculations in lattice QCD by the HPQCD Collaboration. Each of the calculations proceed by generating two- and three-point quark-line connected correlation functions – a standard procedure in lattice QCD – by combining propagators for heavy valence quarks (defining heavy here as being at or above the c quark mass), which are generated from ensembles of gluon field configurations. We use the Highly Improved Staggered Quark (HISQ) formalism [1] for our valence quarks. The configurations we use were provided by the MILC Collaboration [2, 3] and include the effect of $2+1+1$ quarks in the sea using the HISQ formalism. For each calculation we select from lattice spacings that range from ≈ 0.15 fm down to ≈ 0.03 fm. We use two values of the light (u/d) quark masses: either $m_s/m_l = 5$ or m_l takes on its physical value such that the pion has its experimental value.

We will discuss a series of radiative decay calculations using lattice QCD with analogous approaches. First we summarise results from calculations of the two-photon decays $\eta_c \to \gamma\gamma$ and $\eta_b \to \gamma\gamma$. We also explore the mass dependence of this process by looking at the intermediate region $m_b \leq m_h \leq m_c$, using the subscript h to denote heavy quarks, including c and b, generally. Finally, we present recent results from the decay $J/\psi \to \gamma a$ where a is an axion-like particle.

These calculations build on a body of earlier work that includes accurate calculations of meson masses and decay constants and accurate determination of quark masses in lattice QCD+QED [4–6].

2. $\eta_h \to \gamma\gamma$

We recently studied the processes $\eta_h \to \gamma\gamma$ for $h = c, b$ and the two intermediate M_h values 4.0 GeV and 6.62 GeV [7, 8]. The two-photon decay rate is parameterised by the form factor $F(0,0)$, where the two zeroes indicate that both photons in the process are on-shell. It relates to the decay rate through:

$$\Gamma(\eta_h \to \gamma\gamma) = \pi\alpha^2 Q_h^4 M_{\eta_h}^3 (F_{\eta_h}(0,0))^2 \tag{1}$$

where M_{η_h} is the meson mass and Q_h the electric charge of the quark in units of e.

To determine $F(0,0)$ we first construct 3-point correlation functions, shown schematically in Fig. 1. A temporal axial current, coupling to the η_h, is separated from vector current j_μ, located at the time origin, by T. We use several values of $T \geq 0.7$ fm. A second current is inserted at t_{γ_2} with twisted boundary conditions applied to the propagators between the two photons to impart spatial momentum [9, 10]. We set the momentum to be entirely in the y direction, orthogonal to the polarisations of both vector currents, which we choose to be in the x and z directions. The magnitude of the momentum, ω, is set to half the meson mass.

Before fitting, the 3-point correlation function is converted to a 2-point correlation function by summing over all t_{γ_2} from $-L/2+1$ to $L/2-1$ with weight $\exp(-\omega t_{\gamma_2})$:

$$\tilde{C}(T) = \sum_{-L/2+1}^{L/2-1} C(t,T) e^{-\omega t_{\gamma_2}}. \tag{2}$$

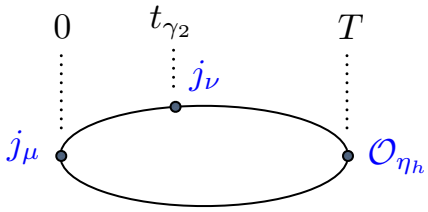

Figure 1: Picture of the set up of our 3-point correlation functions. Operator O_{η_h} is separated by T from vector current j_μ, and a second vector current j_ν coupling to photon γ_2 is inserted at all t_{γ_2}. The lines represent the heavy quark propagators. Spatial momentum is imparted by applying twisted boundary conditions to the propagator between j_μ and j_ν.

This sets photon 2 on-shell [11–13]. We fit $\tilde{C}(T)$ alongside a standard 2-point function between two temporal axial currents, $C(t)$, both to a sum of exponentials,

$$C(t) = \sum_n a_n^2 e^{M_n t}; \quad \tilde{C}(T) = \sum_n a_n b_n e^{-M_n T}, \tag{3}$$

which allows us to isolate the ground-state amplitude b_0. Note that the HISQ formalism results in additional, oscillating terms in the above expressions that we have not shown here but are included in our fit. Using b_0 we can determine the form factor in lattice units:

$$\frac{F(0,0)}{a} = b_0 \sqrt{\frac{2}{aM_{\eta_h}}} \frac{L_s}{\theta\pi} Z_V^2. \tag{4}$$

Z_V is the normalisation factor for the local vector current, which is determined at 2 GeV in the RI-SMOM intermediate scheme [5, 14], θ is the twist angle used to set the momentum and L_s is the number of lattice points in any spatial direction.

2.1 $\eta_c \to \gamma\gamma$

Our first results are for the charmonium case, where we made a significant improvement to the theoretical picture for $\eta_c \to \gamma\gamma$ by making a direct determination of $F(0,0)$ [7]. As part of this study we noted that there is a useful dimensionless ratio that has a simple limit in leading-order nonrelativistic QCD (NRQCD):

$$R = \frac{f_{\eta_h}}{M_{\eta_h}^2 F(0,0)} = \frac{1}{2}\left(1 + O(\alpha_s) + O\left(v^2/c^2\right)\right). \tag{5}$$

Strong mass dependences from the individual quantities are cancelled in this ratio where f and M are a meson decay constant and mass respectively. For R, we fit our lattice data to the form

$$\begin{aligned} R_{\eta_h}^{\text{latt}} = & R_{\eta_h}^{\text{phys}} \left(1 - \frac{q_1^2}{M_{\text{pole}}}\right) \left[1 + \sum_{i=1}^{i_{\max}} \kappa_{a\Lambda}^{(i)} (a\Lambda)^{2i} + \kappa_{\text{val},h}\delta^{\text{val},h} + \kappa_{\text{sea},c}\delta^{\text{sea},c} \right. \\ & \left. + \kappa_{\text{sea},uds}^{(0)}\delta^{\text{sea},uds}\left\{1 + \kappa_{\text{sea},uds}^{(1)}(a\tilde{\Lambda})^2 + \kappa_{\text{sea},uds}^{(2)}(a\tilde{,}\Lambda)^4\right\}\right] \end{aligned} \tag{6}$$

where the $\kappa_{a\Lambda}$ terms allow for discretisation effects from our lattice calculation. The scale Λ is determined using the Empirical Bayes approach where it takes on the value that maximises the

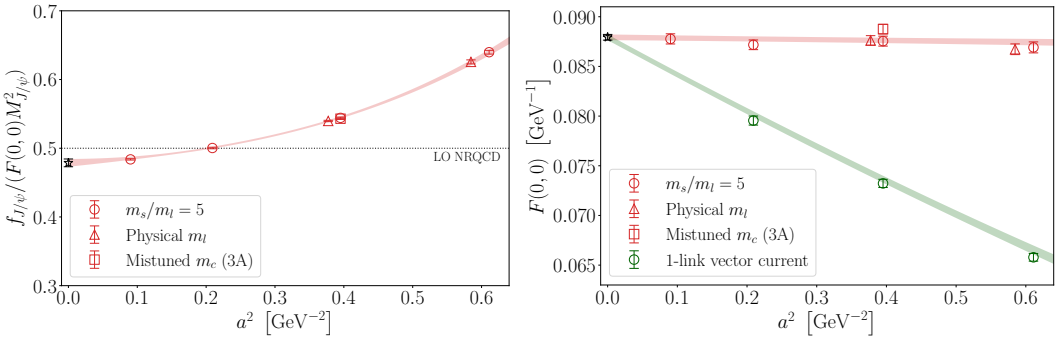

Figure 2: Left: Fit to the ratio $f_{J/\psi}/(M^2_{J/\psi}F(0,0))$ for the process $\eta_c \to \gamma\gamma$. The black star corresponds to the result in the continuum limit at the physical value of m_l. The dotted line is the result in leading order NRQCD. Right: Continuum fit of the form factor $F(0,0)$. The red and green points, and their respective fit bands, correspond to two different sets of operators for $\mathcal{O}_{\eta_c}$, j_μ and j_ν that have different discretisation errors but that give the same result in the continuum limit. The black star shows the continuum result from a joint fit of both sets of operators at the physical light quark mass.

Bayes factor [15]. The δ terms account for the small mistuning of the heavy valence quark, the c quark in the sea and, separately, the $u/d/s$ quarks in the sea. When we perform the weighted sum over time to construct $\tilde{C}(T)$, this places γ_2 exactly on-shell but γ_1 can still be very slightly off-shell. We therefore include the factor $(1 - q_1^2/M^2_{\text{pole}})$ to correct for this. M_{pole} is a fit parameter that we give a prior of M_{η_h} with a width of 10%. Full details of the fit including how the quark masses are tuned and the values chosen for the priors are given in [7].

Figure 2 (left) shows our result for R_{η_c} after fitting to Eq. (6). The square point has a deliberately mistuned charm mass to provide information on valence quark effects for our fit and is labelled (3A) in accordance with the original paper [7]. The black star is our result in the continuum limit at physical quark masses, i.e. where lattice spacing a and δ terms are zero. The dotted line shows the leading order NRQCD result appearing in Eq. (5). The result in the continuum is

$$R_{\eta_c} = 0.4786(57)_{\text{fit}}(14)_{\text{syst}}, \tag{7}$$

where the first uncertainty comes from our fit and the second uncertainty accounts for quark line disconnected correlators and QED effects that have been excluded from our calculation of the form factor $F(0,0)$; these are also discussed in detail in [7].

It should be noted that we take the J/ψ decay constant and mass, $f_{J/\psi}$ and $M_{J/\psi}$, in this ratio and at this order in NRQCD there is no distinction between M_{η_c} and $M_{J/\psi}$. In [8] we carry out a re-analysis using f_{η_c} and M_{η_c} for direct comparison with our study of $\eta_h \to \gamma\gamma$ over a range of m_h values where η_h quantities were used.

Figure 2 (right) gives our result for the direct fit to $F(0,0)$. This uses a fit form analogous to that in Eq. (6), except $(1 - q^2/M^2_{\text{pole}})$ is in the denominator of the right-hand side in this case. The red points and bands map directly to those in the R_{η_c} fit. The points and band labelled '1-link vector current' use an alternative set of operators for $\mathcal{O}_{\eta_c}$, j_μ and j_ν, giving different discretisation errors but the same result in the continuum limit. Both sets of points are fitted simultaneously. The continuum result is depicted by a black star. We find

$$F(0,0) = 0.08793(29)_{\text{fit}}(26)_{\text{syst}}. \tag{8}$$

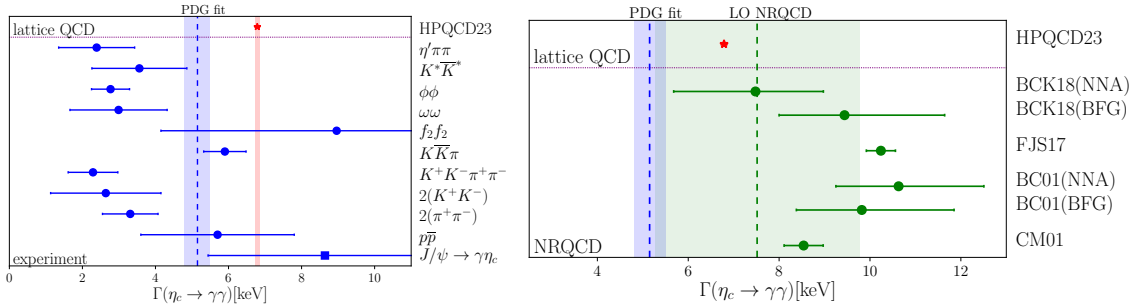

Figure 3: Left: Comparison of our result (red star and band) with results from experiment (see text). The blue dashed line and fit are the PDG fit from [16]. Inconsistencies in the experimental data result in a χ^2 of 118 for 81 degrees of freedom. Right: Comparison of our result (red star) with NRQCD. The green dashed line is the leading order NRQCD result with a ±30% uncertainty band to account for higher order effects. The green circles are results from higher-order calculations (see text). The PDG fit is again shown.

Using $M_{\eta_c} = 2.9839(4)$ GeV and $1/\alpha = 137.036$ [16] in Eq. (1) we determine the decay width as

$$\Gamma(\eta_c \to \gamma\gamma) = 6.788(45)_{\text{fit}}(41)_{\text{syst}} \text{ keV}. \tag{9}$$

The impact of this calculation in full lattice QCD is demonstrated in Fig. 3 where we show two comparisons with other determinations of $\Gamma(\eta_c \to \gamma\gamma)$. On the left plot we compare our result (red star and band) with results from experiment. The blue circles are from determinations of the product $\Gamma(\eta_c \to i)\Gamma(\eta_c \to \gamma\gamma)/\Gamma_{\text{total}}(\eta_c)$ where i is the decay channel listed. The blue square comes from a determination of the product of branching fractions for $J/\psi \to \gamma\eta_c$ and $\eta_c \to \gamma\gamma$ from BESIII [17] alongside $\mathcal{B}(J/\psi \to \gamma\eta_c)$. The blue band shows the result of the PDG fit to this and other data experimental data at the time ref. [16] was written. Tension between the various experimental results becomes clear through the fit quality: it has $\chi^2 = 118$ for 81 degrees of freedom and shows over 4σ tension with our precise theoretical result.

The right-hand plot in Fig. 3 compares our result with NRQCD. The green dashed line shows the leading order NRQCD result, and we add a ±30% uncertainty band to account for higher order corrections. The green points are from various NRQCD calculations that included higher order effects [18–21]. Additional details, including further comparisons with our results, are discussed in [7].

2.2 $\eta_b \to \gamma\gamma$ and heavy mass dependence

We follow an analogous procedure for larger quark masses up to m_b, providing full details in [8]. In this study, however, we perform fits only to the values R_{η_h}. The key result is a prediction of the decay width of the process $\eta_b \to \gamma\gamma$, which is yet to be seen but which should be accessible to Belle II [22]. Our result is the first from a fully relativistic calculation; prior results have relied on nonrelativistic approaches that, since they have missing relativistic and radiative corrections, are limited by their systematic uncertainties. Our calculation is made possible by the use of the HISQ formalism where $O(a^2)$ tree-level lattice artefacts are removed such that discretisation errors first appear at $O(a^4)$. This allows us to reach, and thus avoid the need for an extrapolation to, the physical b quark mass. To explore the mass dependence on the ratio R_{η_h} we also work at the intermediate M_{η_h} values between M_{η_c} and M_{η_b} of 4.0 GeV and 6.62 GeV.

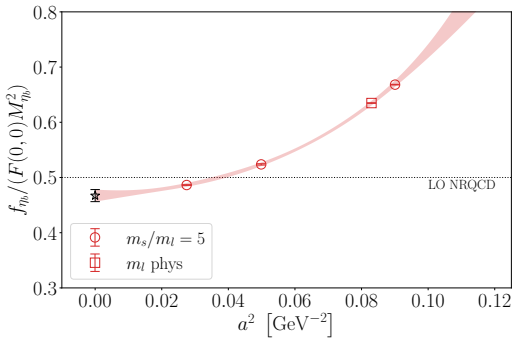

Figure 4: Fit to the ratio $f_{\eta_b}/(M_{\eta_b}^2 F(0,0))$ for the process $\eta_b \to \gamma\gamma$. The black star corresponds to the result in the continuum limit at the physical value of m_l. The dotted line is the result in leading order NRQCD.

The fit form given in Eq. (6) is again used to fit $R_{\eta_h}^{\text{latt}}$ using ensembles of gauge field configurations where the bare quark mass (in lattice units) is $am_h < 1.4$ to keep discretisation effects under control. We use decay constants and masses from the pseudoscalar mesons, f_{η_h} and M_{η_h}. The values of these quantities come from the simultaneous fit to the two sets of correlations functions (see Eq. (3)). The exception is in our reanalysis of $\eta_c \to \gamma\gamma$ where we construct R_{η_c} from the value of $F(0,0)$ from [7] alongside the decay constants and masses extracted from new fits to $C_{\eta_c}(t)$ on each ensemble.

The result for the physical process $\eta_b \to \gamma\gamma$ is plotted in Fig. 4. The fit is given by the red band for physical quark masses, while the black star is again the result in the continuum limit. This corresponds to values of

$$R_{\eta_b} = 0.4674(109); \quad F(0,0)_{\eta_b} = 0.01754(50)\ \text{GeV}^{-1}, \tag{10}$$

where we use the lattice QCD η_b decay constant value 724(12) MeV [5] alongside the experimental η_b mass [23] to obtain the form factor from R_{η_b}. Using Eq. (1) with $1/\alpha = 133.1$[1] we find

$$\Gamma(\eta_b \to \gamma\gamma) = 0.559(32)_{\text{fit}}(1)_{\text{syst}}\ \text{keV}, \tag{11}$$

where the systematic uncertainty comes from missing higher-order QED effects that are known to be small [5]. In contrast with the $\eta_c \to \gamma\gamma$ process, the missing quark-line disconnected diagrams are expected to have a negligible impact on the uncertainty in this case [8].

Figure 5 (left) shows the mass dependence of the ratio R using $M_h = M_{\eta_b}$, 6.62 GeV, 4.0 GeV and M_{η_c}. The two intermediate values were determined in the very same way as R_{η_b}. Results for all masses are (surprisingly) close to the leading-order NRQCD value, but there is a clear trend with R_{η_h} increasing as M_{η_h} falls.

Our result of the partial decay width given in Eq. (11) can be used to make a determination of the total width $\Gamma(\eta_b)$ by combining it with branching fractions determined using NRQCD factorisation. We provide multiple values for the width:

$$\Gamma(\eta_b) = 12.97\left(^{+45}_{-50}\right)^{\text{NNA}}_{\text{BCK18}}(74)_{\text{LQCD}}\ \text{keV}; \quad \Gamma(\eta_b) = 13.47\left(^{+50}_{-56}\right)^{\text{BFG}}_{\text{BCK18}}(77)_{\text{LQCD}}\ \text{keV}; \tag{12}$$

$$\Gamma(\eta_b) = 13.81\left(^{+17}_{-28}\right)^{\text{NNA}}_{\text{RGZ23}}(79)_{\text{LQCD}}\ \text{keV}; \quad \Gamma(\eta_b) = 14.42\left(^{+11}_{-28}\right)^{\text{BFG}}_{\text{RGZ23}}(83)_{\text{LQCD}}\ \text{keV}. \tag{13}$$

[1] This uses the Brodsky-Lepage-Mackenzie scale-setting procedure [24], and we're taking the scale $\alpha = 0.26 M_{\eta_b}$.

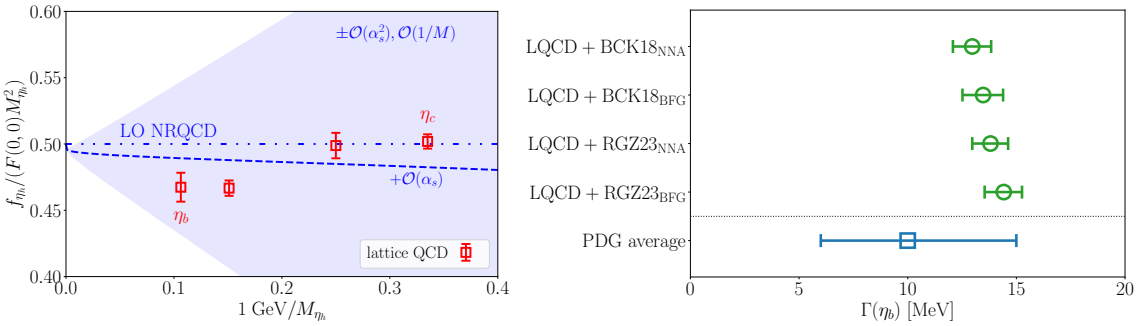

Figure 5: Left: Mass dependence of the ratio $f/(M^2F(0,0))$. For comparison with the lattice QCD results (red squares) we show the leading-order NRQCD result of 0.5 as a dash-dotted line. The dashed line adds in $O(\alpha_s)$ corrections and the blue band adds a relative uncertainty of ± 1 GeV$/M$ to account for missing $O(v^2/c^2)$ corrections. Right: Comparison of inclusive width of η_b from combining the width for $\Gamma(\eta_b \to \gamma\gamma)$ from our lattice QCD calculation with potential NRQCD determinations of $\Gamma(\eta_b)/\Gamma(\eta_b \to \gamma\gamma)$ (green circles). The PDG value is shown as a blue square [23].

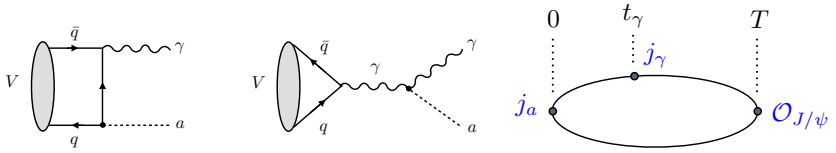

Figure 6: Left and centre: Diagrams that contribute to $V \to \gamma a$ for heavyonium vector meson, V, such as J/ψ discussed here. We calculate the left-hand diagram where the ALP couples to $q\bar{q}$. Right: Schematic of the set up for the 3-point correlator in this calculation.

The values in Eq. (12) use the branching fraction from [21] where the authors used the naive non-abelianisation (NNA) approach and the background-field gauge (BFG) method respectively. The values in Eq. (13) improve on the first two by including color-octet matrix elements that are calculated in the refined Gribov-Zwanziger (RGZ) theory [25]. The first uncertainty in each case comes from the NRQCD factorisation approach, and the second is from our result. All values are consistent with the experimental average, $\Gamma(\eta_b) = 10^{+5}_{-4}$ MeV [23], but are more accurate. We compare the values in Fig. 5 (right).

3. $J/\psi \to \gamma a$

For the first time in lattice QCD we have provided form factors for the decay $J/\psi \to \gamma a$, where a is an axion-like particle (ALP), through the $ac\bar{c}$ coupling. ALPs are pseudo Nambu-Goldstone bosons appearing in extensions to the Standard Model and are associated with global symmetry breaking [26]. The two possible diagrams that contribute to this decay are shown as the left and centre pictures in Fig. 6. The leftmost diagram is what we calculate in lattice QCD, again using the HISQ formalism for all quarks.

In this process the full decay width, including both diagrams, is

$$\Gamma(J/\psi \to \gamma a) = \frac{\alpha Q_c^2 M_{J/\psi}^3}{24 f_a^2}\left(1 - \frac{m_a^2}{M_{J/\psi}^2}\right) \times \left| c_{cc}(\mu)\tilde{F} - c_{\gamma\gamma}\frac{\alpha}{\pi}\frac{f_{J/\psi}}{M_{J/\psi}}\left(1 - \frac{m_a^2}{M_{J/\psi}^2}\right)\right|^2, \quad (14)$$

where we define

$$\tilde{F} \equiv \frac{2m_c}{M_{J/\psi}} F(0, m_a) \left(1 - \frac{m_a^2}{M_{J/\psi}^2}\right) \tag{15}$$

allowing a comparison with the form factor, $F(0, m_a)$, that we calculate on the lattice with $\tilde{F}$ from perturbation theory. The scale dependence of the dimensionless effective couplings c_{cc} and $c_{\gamma\gamma}$ are discussed in [26].

The set up of this calculation is analogous to the $\eta_h \to \gamma\gamma$ decays but for the currents in the fixed positions as shown on the right of Fig. 6. This time an operator $O_{J/\psi}$ is separated from a local pseudoscalar current j_a – coupling to the ALP – by T, while a local vector current j_γ is inserted at all t_γ. This time it is the polarisations of the J/ψ and photon that are set orthogonally in the x and z directions so that the momentum inserted via twisted boundary conditions can again be arranged in the y direction between j_a and j_γ. For an on-shell photon and ALP we insert the spatial momentum

$$|\mathbf{q}| = \frac{M_{J/\psi}}{2} \left(1 - \frac{m_a^2}{M_{J/\psi}^2}\right), \tag{16}$$

to give values of m_a = 0,1, 2 and 2.5 GeV using the experimental value of the J/ψ mass to fix $m_a/M_{J/\psi}$. The tuning of the momentum $|\mathbf{q}|$ can be done very accurately because our valence charm quark masses are tuned to give a J/ψ mass equal to the experimental value [4].

The 3-point correlation function is converted to a 2-point correlation function by again performing a weighted sum over the lattice time slices as in Eq. (2). Then, fitting this 2-point function with the standard 2-point correlation function between two $O_{J/\psi}$ operators (see Eq. (3)) we can extract ground-state amplitude b_0 to determine

$$F_{\text{latt}} = b_0 \frac{\sqrt{2aM_{J/\psi}}}{aq^y}. \tag{17}$$

After inserting normalisation factors and simplifying for our momentum configuration, discussed in [27], we obtain the form factor

$$\tilde{F}_{\text{latt}} = Z_V b_0 \sqrt{2aM_{J/\psi}} \frac{4am_c^{\text{val}}}{(aM_{J/\psi})^2}, \tag{18}$$

which we can compare with perturbation theory. In this equation, am_c^{val} is the valence charm quark mass, in lattice units, that is an input to our calculation.

Having generated lattice data for four values of m_a on multiple ensembles[2], and at physical and heavier-than-physical light quark masses, we want to determine the form factor at physical quark masses in the continuum limit while interpolating between ALP masses. To achieve this, we fit to the following form:

$$\begin{aligned}\tilde{F}_{\text{latt}}(a, X, m_q) &= S_0(X) + \sum_{i=1}^{i_{\max}} \kappa_{am_c}^{(i)} (am_c)^{2i} S_1^{(i)}(X) + \kappa_{\text{val},c} S_2(X) \delta_c^{\text{val}} + \kappa_{\text{sea},c} S_3(X) \delta_c^{\text{sea}} \\ &+ \kappa_{\text{sea},uds}^{(0)} \delta_{uds}^{\text{sea}} \left\{ S_4^{(0)}(X) + \kappa_{\text{sea},uds}^{(1)} (am_c)^2 S_4^{(1)}(X) + \kappa_{\text{sea},uds}^{(2)} (am_c)^4 S_4^{(2)}(X) \right\}, \end{aligned} \tag{19}$$

[2]On our ensemble with the finest lattice spacing, we include two additional m_a values close to 1 GeV and 2 GeV.

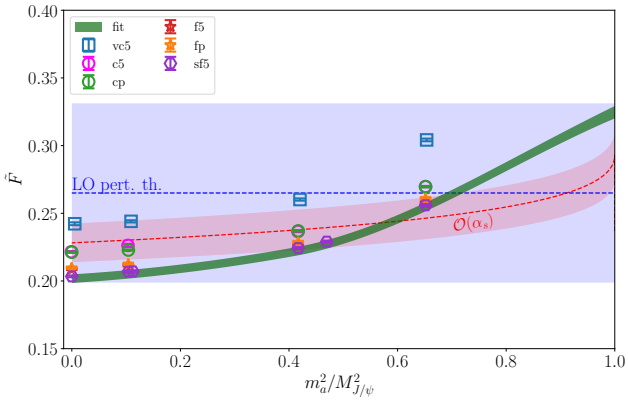

Figure 7: The form factor $\tilde{F}$ as a function of the ratio $m_a^2/M_{J/\psi}^2$. The points show the lattice data on each of the ensembles used (the labels in the legend correspond to those in [27]) while the green band is a fit to this data using cubic splines as discussed in the text, giving the continuum result for physical quark masses. The blue and red dashed lines with their corresponding bands show the NRQCD perturbation theory prediction at leading order and including $O(\alpha_s)$ corrections, respectively.

where $X \equiv m_a^2/M_{J/\psi}^2$ $(0 < X < 1)$, and $S_n(X)$ are cubic splines. We use Steffen splines [28] since they are monotonic between points. The leading spline $S_0(X)$ gives the result in the continuum limit with all quarks set to their physical values. To determine X for each point we use the value of $M_{J/\psi}$ from our correlation function fits and our input value of the twist, θ:

$$X = 1 - \frac{2\pi\theta}{aM_{J/\psi}L_s}. \tag{20}$$

The δ terms again account for slight mistunings of the quarks on our lattice ensembles and full details on how they are determined are given in [27].

Figure 7 shows our result for $\tilde{F}$ from lattice QCD as a function of $m_a^2/M_{J/\psi}^2$ alongside results from leading-order and next-to-leading-order nonrelativistic perturbation theory [27]. The points and green band are the lattice data and result of the cubic spline fit in the continuum limit. The blue dashed line gives the leading order perturbation theory result with a 25% uncertainty band to account for missing $O(\alpha_s)$ effects, while the red dashed line and band give the result at first-order with uncertainty $1 \times [\alpha_s(M_{J/\psi})]^2$. The shape of the first-order perturbation theory result is qualitatively better at reproducing the curve of the X-dependence from lattice QCD than the flat leading-order result, but the values of $\tilde{F}$ are still not in good agreement, suggesting that missing higher order corrections are sizeable. The lattice QCD result, which includes relativistic effects not present in the perturbative calculation, should therefore be preferred when setting ALP constraints.

Our calculation of $\tilde{F}$ in lattice QCD can be used to place constraints on the ALP parameter space. Figure 8 (left) shows the branching fraction for an ALP that couples only to charm quarks normalised by the coupling $c_{cc}(\mu_c)$ and the ALP decay constant f_a, determined by setting $c_{\gamma\gamma} = 0$ in Eq. (14) and dividing by the total width of the J/ψ from experiment. The green band uses our lattice QCD result for $\tilde{F}$, while the blue and red bands are the leading-order and next-to-leading order results from perturbation theory respectively. Our lattice QCD result lies below the values obtained using perturbation theory for most of the mass region indicating that perturbative theory is overestimating the branching ratio.

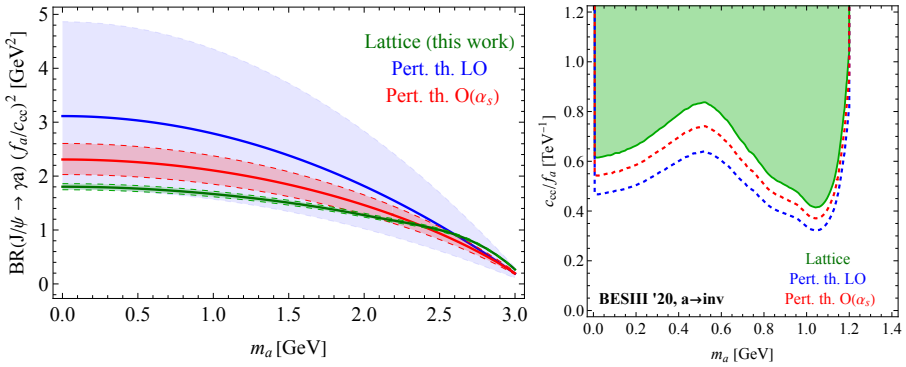

Figure 8: Left: Branching ratio for J/ψ where an ALP is coupled only to charm quarks, normalised by $(f_a/c_{cc})^2$. The result using our lattice QCD result is shown in green. The blue and red curves show leading-order and $O(\alpha_s)$ results calculated in the perturbative approach respectively. Right: Constraints on ALP parameters space using a BESIII search for $J/\psi \to \gamma +$ invisible. The green region uses our lattice QCD results. The blue and red dashed lines give the central values of the boundary of the exclusion region using the perturbative calculation.

These results can further be combined with the search for $J/\psi \to \gamma +$ invisible by BESIII [29]. This process is sensitive to ALPs in the mass range $m_a < 1.2$ GeV that are stable relative to the size of detectors, which is the case for ALPs that couple only to charm quarks. The coupling c_{cc} is also effectively a scale-invariant quantity in this process because its self-renormalisation is proportional to the square of the small charm Yukawa [27]. This allows for upper limits to be placed as shown in Fig. 8 (right) where we combine the branching ratio from the left-hand plot and the BESIII result for the upper limit of the J/ψ branching fraction at each value of the ALP mass at 90% confidence level. The green excluded region again uses our lattice QCD result from [27] while the blue and red dashed lines use the results from leading-order and $O(\alpha_s)$ results from the perturbative approach.

In [27] we provide further constraints for different scenarios for the interested reader. For example, we consider cases where $J/\psi \to \gamma a$ proceeds through *both* possible paths shown in Fig. 6 where the model has flavour universal couplings to up-type quarks at scale Λ, alongside tree level couplings to photons for a selection of ALP masses.

4. Conclusions

In these proceedings we have presented some recent results from work on radiative heavyonium decays. These calculations include the first accurate results for an observed process ($\eta_c \to \gamma\gamma$), make Standard Model predictions ($\eta_b \to \gamma\gamma$) and provide exclusion regions for parameter spaces in Beyond the Standard Model physics ($J/\psi \to \gamma a$). They, of course, represent only a sample of the recent heavyonium results from lattice QCD that include further improvements to charmonium decays (such as $J/\psi \to \eta_c\gamma$ and the Dalitz decay $J/\psi \to \eta_c e^+e^-$) as well as studies of meson masses and decay constants that include the effect of (quenched) QED on the lattice [4–6]. The lattice QCD calculations described here are also readily extended to other processes such as ALP searches in $\Upsilon \to \gamma a$, which covers a larger range of ALP masses than J/ψ by working at b quark masses using the same techniques described here, and charged pseudoscalar leptonic decays with ALP radiation such as $B \to \ell\bar{\nu}a$ or $D_s \to \ell\bar{\nu}a$.

Acknowledgments

We thank the MILC collaboration for making publicly available their gauge configurations and their code, MILC-7.7.11 [30]. This work used the DiRAC Data Intensive Service (CSD3) at the University of Cambridge, managed by the University of Cambridge Information Services on behalf of the Science and Technology Facilities Council (STFC) DiRAC HPC Facility (www.dirac.ac.uk). The DiRAC component of CSD3 at Cambridge was funded by BEIS, UKRI and STFC capital funding and STFC operations grants. DiRAC is part of the UKRI Digit Research Infrastructure. We are grateful to the CSD3 support staff for assistance. This work was funded by STFC grant ST/T000945/1. SR is supported by UKRI Stephen Hawing Fellowship EP/W005433/1. The bibliography was partially compiled using *filltex* [31].

References

[1] E. Follana, Q. Mason, C. Davies, K. Hornbostel, G.P. Lepage, J. Shigemitsu et al., *Highly improved staggered quarks on the lattice, with applications to charm physics*, *Phys. Rev. D* **75** (2007) 054502 [hep-lat/0610092].

[2] A. Bazavov et al., *Scaling studies of QCD with the dynamical HISQ action*, *Phys. Rev. D* **82** (2010) 074501 [1004.0342].

[3] A. Bazavov et al., *Lattice QCD Ensembles with Four Flavors of Highly Improved Staggered Quarks*, *Phys. Rev. D* **87** (2013) 054505 [1212.4768].

[4] D. Hatton, C.T.H. Davies, B. Galloway, J. Koponen, G.P. Lepage and A.T. Lytle, *Charmonium properties from lattice QCD+QED : Hyperfine splitting, J/ψ leptonic width, charm quark mass, and a_μ^c*, *Phys. Rev. D* **102** (2020) 054511 [2005.01845].

[5] D. Hatton, C.T.H. Davies, J. Koponen, G.P. Lepage and A.T. Lytle, *Bottomonium precision tests from full lattice QCD: Hyperfine splitting, Υ leptonic width, and b quark contribution to $e^+e^- \to$ hadrons*, *Phys. Rev. D* **103** (2021) 054512 [2101.08103].

[6] D. Hatton, C.T.H. Davies, J. Koponen, G.P. Lepage and A.T. Lytle, *Determination of $\overline{m}_b/\overline{m}_c$ and $\overline{m}_b$ from $n_f = 4$ lattice QCD+QED*, *Phys. Rev. D* **103** (2021) 114508 [2102.09609].

[7] B. Colquhoun, L.J. Cooper, C.T.H. Davies and G.P. Lepage, *Precise determination of decay rates for $\eta_c \to \gamma\gamma$, $J/\psi \to \gamma\eta_c$, and $J/\psi \to \eta_c e^+e^-$ from lattice QCD*, *Phys. Rev. D* **108** (2023) 014513 [2305.06231].

[8] B. Colquhoun, C.T.H. Davies and G.P. Lepage, *Precise prediction of the decay rate for $\eta_b \to \gamma\gamma$ from lattice QCD*, 2410.24041.

[9] C.T. Sachrajda and G. Villadoro, *Twisted boundary conditions in lattice simulations*, *Phys. Lett. B* **609** (2005) 73 [hep-lat/0411033].

[10] D. Guadagnoli, F. Mescia and S. Simula, *Lattice study of semileptonic form-factors with twisted boundary conditions*, *Phys. Rev. D* **73** (2006) 114504 [hep-lat/0512020].

[11] X.-d. Ji and C.-w. Jung, *Studying hadronic structure of the photon in lattice QCD*, *Phys. Rev. Lett.* **86** (2001) 208 [hep-lat/0101014].

[12] X.-d. Ji and C.-w. Jung, *Photon structure functions from quenched lattice QCD*, *Phys. Rev. D* **64** (2001) 034506 [hep-lat/0103007].

[13] J.J. Dudek, R.G. Edwards and D.G. Richards, *Radiative transitions in charmonium from lattice QCD*, *Phys. Rev. D* **73** (2006) 074507 [hep-ph/0601137].

[14] D. Hatton, C.T.H. Davies, G.P. Lepage and A.T. Lytle, *Renormalizing vector currents in lattice QCD using momentum-subtraction schemes*, *Phys. Rev. D* **100** (2019) 114513 [1909.00756].

[15] G.P. Lepage, B. Clark, C.T.H. Davies, K. Hornbostel, P.B. Mackenzie, C. Morningstar et al., *Constrained curve fitting*, *Nucl. Phys. B Proc. Suppl.* **106** (2002) 12 [hep-lat/0110175].

[16] R.L. Workman et al., *Review of Particle Physics*, *PTEP* **2022** (2022) 083C01.

[17] M. Ablikim et al., *Evidence for $\eta_c \to \gamma\gamma$ and measurement of $J/\psi \to 3\gamma$*, *Phys. Rev. D* **87** (2013) 032003 [1208.1461].

[18] A. Czarnecki and K. Melnikov, *Charmonium decays: J / psi —> e+ e- and eta(c) —> gamma gamma*, *Phys. Lett. B* **519** (2001) 212 [hep-ph/0109054].

[19] F. Feng, Y. Jia and W.-L. Sang, *Next-to-Next-to-Leading-Order QCD Corrections to the Hadronic width of Pseudoscalar Quarkonium*, *Phys. Rev. Lett.* **119** (2017) 252001 [1707.05758].

[20] G.T. Bodwin and Y.-Q. Chen, *Resummation of QCD corrections to the eta(c) decay rate*, *Phys. Rev. D* **64** (2001) 114008 [hep-ph/0106095].

[21] N. Brambilla, H.S. Chung and J. Komijani, *Inclusive decays of η_c and η_b at NNLO with large n_f resummation*, *Phys. Rev. D* **98** (2018) 114020 [1810.02586].

[22] J.S. Lange and E. Prencipe, *Hadron Spectroscopy: The next big steps, workshop at Mainz Institute for Theoretical Physics* (2022) .

[23] S. Navas et al., *Review of particle physics*, *Phys. Rev. D* **110** (2024) 030001.

[24] S.J. Brodsky, G.P. Lepage and P.B. Mackenzie, *On the Elimination of Scale Ambiguities in Perturbative Quantum Chromodynamics*, *Phys. Rev. D* **28** (1983) 228.

[25] H.S. Chung, *Color-octet nonrelativistic QCD matrix elements for heavy quarkonium decays in the refined Gribov-Zwanziger theory*, *Phys. Rev. D* **109** (2024) 054001 [2312.10601].

[26] M. Bauer, M. Neubert, S. Renner, M. Schnubel and A. Thamm, *Flavor probes of axion-like particles*, *JHEP* **09** (2022) 056 [2110.10698].

[27] B. Colquhoun, C.T.H. Davies, G.P. Lepage and S. Renner, *Constraints on axion-like particles using lattice QCD calculations of the rate for $J/\psi \to \gamma a$*, *Phys. Rev. D* **111** (2025) 114513 [2502.06721].

[28] M. Steffen, *A simple method for monotonic interpolation in one dimension.*, *Astron. Astrophys.* **239** (1990) 443.

[29] M. Ablikim et al., *Search for the decay $J/\psi \to \gamma +$ invisible*, *Phys. Rev. D* **101** (2020) 112005 [2003.05594].

[30] MILC, *code repository*, https://github.com/milc-qcd.

[31] D. Gerosa and M. Vallisneri, *filltex: Automatic queries to ADS and INSPIRE databases to fill LaTex bibliography*, *The Journal of Open Source Software* **2** (2017) 222.